Journal of Materials Chemistry C

ARTICLE

Synthesis of Planar Dibenzo[*de, op*]bistetracene Derivatives for Organic Field-effect Transistors Applications: Substituent Effect on Crystal Packing and Charge Transport Property

Tien-Lin Wu,[a] Chi-Hsien Kuo,[b] Bo-Chao Lin,[b] Yu-Tai Tao[a,b],* Chao-Ping Hsu,[b],*and Rai-Shung Liu[a],*

A series of substituted dibenzo[*de, op*]bistetracenes (DBBTs) is prepared in short steps and their applications to organic field-effect transistors (OFETs) are described. These DBBT derivatives bear one or two methyl-, *tert*-butyl-, or fluoro groups at the 2-, 10-positions. X-ray diffraction studies reveal that the molecular structures of these DBBTs were planar with a shifted π–π stacking or herringbone-stacked type packing in the crystalline state. These substituents perturb the degree of stacking shift because of steric effect and dipolar interaction, consequently affecting the electronic coupling between the neighboring molecules. Needle-like single crystals of DBBT derivatives were prepared by vapor phase transfer method and used for the fabrication of single-crystal field-effect transistors (SCFETs). Theoretical calculation on these DBBTs has been performed to correlate the measured field-effect mobility with their molecular packing. The SCFET of di-methyl derivative **4b** showed the highest hole mobility (1.19 cm^2 V^{-1} s^{-1}) with a current on/off ratio of 10^6.

Introduction

In recent two decades, polycyclic aromatic hydrocarbons (PAHs) have been extensively studied as organic materials in various electronic devices such as organic light-emitting diodes (OLEDs),[1] organic field-effect transistors (OFETs) [2-4], organic solar cells and etc. The development of these materials facilitates the advancement of flexible, low-cost and light-weight electronics.[3] Small and medium size PAHs become attractive materials because of their high oxidation resistance, carrier mobility, and photoluminescent properties, besides their amenability to rational synthesis.[1-4] The high charge mobility of these PAHs may be ascribed to the potential of extensive overlap of the conjugate π systems and thus higher electronic coupling, and lower reorganization energies due to disperse of charge over the conjugate system. Both higher electronic coupling and lower reorganization energy are believed to be beneficial to charge transport between molecules.[5] Single crystal field-effect transistors (SCFETs) have often been used to explore the genuine transport characteristics of organic materials because

defects, grain boundaries typically associated with polycrystalline films can be excluded. For instance, linear acenes including anthracene,[6] tetracene[7] and pentacene[8] exhibited high charge mobility. Among these linear-shape PAHs, pentacene derivatives are especially notable because of their large charge-carrier mobility (15−40 cm^2 V^{-1} s^{-1}) with a current on/off ratio of up to 10^6, reported by Palstra et al.[8a] In addition, there is important achievement for two-dimensional shaped PAHs, such as coronenes,[9] triphenylenes,[10] rylenes[11] and graphene nanoribbons (GNR).[12] For coronene derivatives like hexbenzocoronenes (HBCs)[9a-c] and tetrabenzocoronenes (TBCs),[9d-f] the former exhibits discotic structures comprising 2D column packing structures; the latter show contorted structure to contain co-facial or shifted π–π packing states, resulting in good hole mobility of 1.19 cm^2 V^{-1} s^{-1} in SCFET devices.[9f] Thus searching for new polyaromatic molecules suitable for transistor application is of current interest.

Dibenzo[*de, op*]bistetracene (DBBT, **4a**) is a polyaromatic molecules with ten ring fused together. It was first synthesized by Zinke via a long procedure.[13] We recently developed a short synthesis of DBBT derivative **4e** (Figure 1).[14] Notably, the medium-sized π-plane of DBBT **4a** is shown to be quite planar as that of coronene derivatives,[9] thus enabling packing with a neighboring molecule in any direction. Furthermore, such molecules are not fully sextets with significant double bond character that is intrinsically

[a.] *Department of Chemistry, National Tsing Hua University, Hsin-Chu, Taiwan*
[b.] *Institute of Chemistry, Academia Sinica, Taipei, Taiwan*

This journal is © The Royal Society of Chemistry 20xx

J. Mater. Chem. C, 2015, **00**, 1-3 | **1**

favored for electronic coupling. We thus undertook a study of the effect of substituents on the molecular packing and thus the charge carrier mobility as measured by their SCFET devices. Herein, we synthesized unsubstituted DBBT **4a** together with symmetrically substituted DBBTs **4b-4c** ($R^1 = R^2 = $ Me, F) and **4e** ($R^1 = R^2 = $ *t*-butyl), and one unsymmetrical derivative **4d** ($R^1 = $ Me, $R^2 = $H). Photophysical properties as well as crystal structures were determined for all five derivatives. Single crystal field-effect transistors were fabricated and mobility measured. One representative compound **4b** exhibited outstanding hole mobility 1.19 cm^2 V^{-1} s^{-1} with a current on/off ratio of up to 10^6. Theoretical calculations are performed to provide rationales for the mobility/molecular packing correlation.
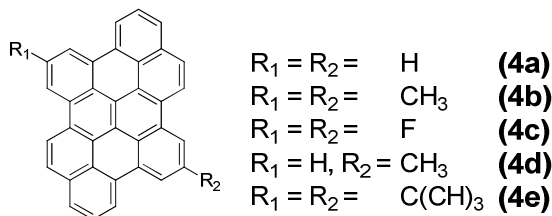

$R_1 = R_2 =$	H	**(4a)**
$R_1 = R_2 =$	CH_3	**(4b)**
$R_1 = R_2 =$	F	**(4c)**
$R_1 = H, R_2 =$	CH_3	**(4d)**
$R_1 = R_2 =$	$C(CH)_3$	**(4e)**

Figure 1. Structure of dibenzo[*de, op*]bistetracene studied.

Results and discussion

Synthesis and Characterization

We previously reported the synthesis of dibenzo[*de,op*]bistetracene (DBBT) derivative **4e** through the Scholl oxidation of dibenzochrysene derivatives.[14] Here, the same procedure was applied to the synthesis of parent DBBT and other derivatives **4a-4d**, with a synthetic protocol shown in Scheme 1. An initial Suzuki coupling reaction[15] of 1,2-bis(2-bromophenyl)ethyne derivatives with naphthalen-2-ylboronic acid (2.1 equiv), K_2CO_3 (6 equiv) and $Pd(PPh_3)_4$ (4 mmol %) in mixed solvents, EtOH/toluene/H_2O, yielded products **1a-1e** in 55−84% yield. Treatment of these coupling products with ICl (1.3 equiv) in cold dichloromethane (-30 °C) afforded iodo derivatives **2a-2e** in 70−82% yields. Mizoroki-Heck coupling reactions[16] of these iodo species **2a-2e** with Na_2CO_3 (4 equiv) and $Pd(PPh_3)_2Cl_2$ (5 mmol %) in dimethylacetamide gave dibenzochrysene derivatives **3a-3e** in 36−71% yield. Here, the unsymmetrical form **2d** existed in two stereoisomers due to the presence of two nonplanar fjord regions; the isomers were inseparable by column chromatography. DDQ-oxidation (DDQ = 2,3-dichloro-5,6-dicyanobenzoquinone)[17] of compounds **3a-3e** in cold dichloromethane (0 °C), afforded the desired DBBTs **4a-4e** in 51−91% yield. Each step in this reaction sequence proceeded with good efficiency, except for fluorinated derivative **4c**, with low yields in all steps. Final products **4a-4d** were sparingly soluble in common organic solvents and further purified by vacuum sublimation to give yellow to orange solids.

Scheme 1. Synthetic Route toward Compound **4a-4e**

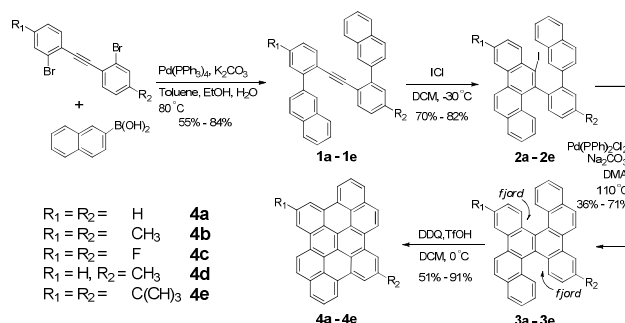| $R_1 = R_2 =$ | H | **4a** |
$R_1 = R_2 =$	CH_3	**4b**
$R_1 = R_2 =$	F	**4c**
$R_1 = H, R_2 =$	CH_3	**4d**
$R_1 = R_2 =$	$C(CH_3)_3$	**4e**

Figure 2 shows the UV-Vis absorption spectra of compounds **4a-4e** in chlorobenzene. All five compounds gave prominent peaks in the 329−333 nm and 483−487 nm regions, assignable to *β*-band and *para*-band (π to π* transition). The HOMO energy levels for all compounds were determined by photoelectron spectrometer (AC2) in the solid state, as listed in Table 1. For these derivatives, their HOMO levels range from 5.27 to 5.51 eV, and their LUMO levels lie within 2.79−3.06 eV. Compounds **4b**, **4d** and **4e** bearing alkyl substituents have both HOMO and LUMO levels higher than those of unsubstituted **4a**. In contrast, the fluoro-substituted **4c** has HOMO similar to its parent species **4a** yet lower LUMO level than the parent compound. Thermal gravimetric analyses (TGA) show that compounds **4a-4d** have excellent thermal stability with decomposition temperature (5% weight loss) at around 490 °C, whereas the bulky *tert*-butyl substituted species **4e** is relatively thermally unstable, decomposing at 303 °C.

Table 1. Photophysical and thermal Properties of Compounds **4a-4e**

Compound	Abs$_{max}$^{a} (nm)	HOMO/LUMO^b (eV)	Band gap^c (eV)	T_d^{d} (°C)
4a	316, 330, 423, 452, 483	5.51/2.99	2.52	491
4b	319, 332, 429, 455, 486	5.39/2.89	2.50	472
4c	315, 329, 431, 456, 487	5.51/3.06	2.45	494
4d	318, 331, 426, 454, 484	5.44/2.94	2.50	494
4e	324, 333, 426, 452, 483	5.27/2.79	2.48	303

^{a} In chlorobenzene, 1.0 x 10^{-5} M. ^{b} The energy levels HOMO are determined from AC2. ^{c} Band gaps were calculated from UV/vis absorption. ^{d} Determined from TGA.
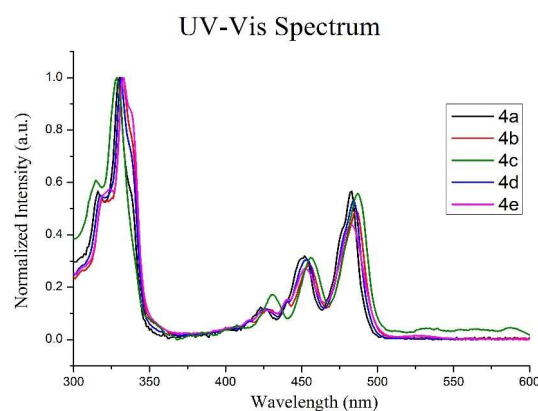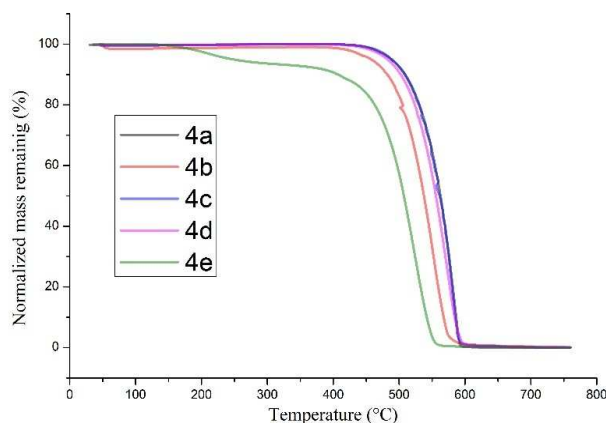
UV-Vis Spectrum

2 | *J. Mater. Chem. C*, 2015, **00**, 1-3

This journal is © The Royal Society of Chemistry 2015

Figure 2. Absorption spectra of compounds **4a-4e**.

Figure 3. Thermal gravimetric analysis of **4a-4e**.

Figure 4. (a) ORTEP drawing of single crystal structure **4a.** (b) ORTEP drawing of single crystal structure **4e.** (c) Crystal packing of **4a** viewing down the molecular axis (*a* axis) and from the top of the molecules (*b* axis) respectively. (d) Crystal packing of **4e** and from the top of the molecules (*b* axis) respectively.

Crystal structure analyses and SCFET properties

Single crystals of DBBT derivatives were grown by physical vapor transport (PVT) method[18] and all five compounds give needle-like crystals. X-ray analyses showed that the core structure of DBBT is nearly flat regardless of the substituents. The ORTEP drawings of **4a** and **4e** (Figure 4) show a planar and symmetrical structure. Compound **4a** packed in a P2$_1$/c space group, showing a shifted π-π stacking when viewed along *b* axis whereas a herringbone type arrangement is observed when viewed along *a* axis. It is suggested the π-π stacking is more significant along *b* axis and this is also the long axis of crystal needles, as indexed from x-ray diffraction. The introduction of substituents results in some minor perturbation on the packing of in compounds **4c** and **4d**, which maintain P2$_1$/c packing motif. The **4b** adopt a orthorhombic Pbca packing motif, whereas more perturbation was observed for **4e**, which now has a C2/c packing motif. They nevertheless all have a shifted π-π stacking direction which is along the direction of the long crystal axis. Selected cell parameters are listed in Table 2.
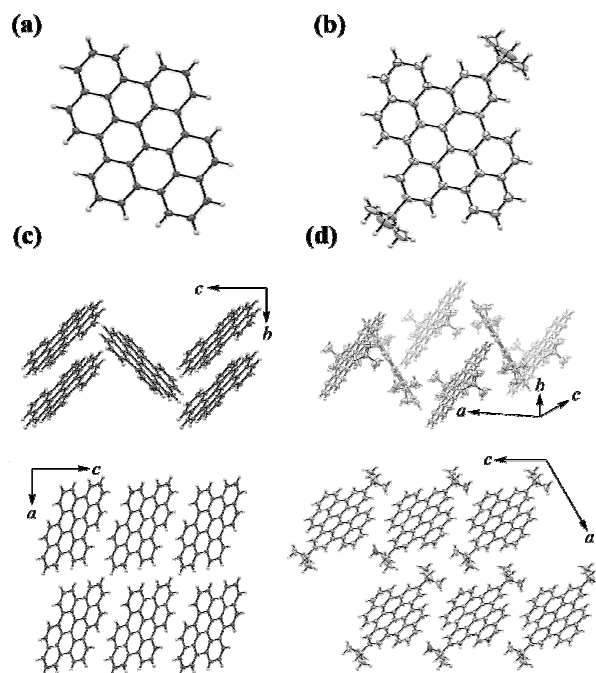
Crystallites obtained from PVT growth were carefully examined under optical microscope for their integrity and then chosen for

device fabrication. Measurements were carried out along the long axes of the crystalline needles, which were indexed to be the (010) plane, i.e. the π-π stacking direction. Figure 5 shows the device structure diagram of a top-gate SCFET with detailed description provided in experimental section. The typical output and transfer characteristic for compound 4a are shown in Figure 6. (Other output and transfer characteristics are shown in supplementary information) The single crystal field-effect transistors were prepared in the same fashion for all compounds, which exhibited typical p-type behavior. Six to eight samples for each compound were prepared and measured. The analyzed device characteristics are summarized in Table 3. Highest mobility was observed for **4b**, at 1.19 cm^2 V^{-1} s^{-1}. An average of 0.83 cm^{2}V^{-1}s^{-1} was obtained for this compound, which is comparable to that for **4c**. Lowest mobility was observed for **4e**, at 0.077 cm^2 V^{-1}s^{-1}. Thus intuitively it seems the introduction of bulky t-butyl substituent pushes away the neighboring molecules and reduces the charge transport rate. An examination of the π-π distance shows 3.37 Å for **4a** and 3.41 Å for **4e**. However, the theoretical calculation suggests otherwise, as will be seen below.

Table 3. SCFET performance of DBBT derivatives

Compound	Mobility (μ, cm^{2}V^{-1}s^{-1})	Average Mobility (μ$_{avg}$)	On / off ratio	Threshold Voltage (V$_{th}$, V)
4a	0.099 - 0.15	0.12 ± 0.018	1 x 10^3 ~ 1 x 10^5	-27 ~ (-48)
4b	0.56 - 1.19	0.83 ± 0.24	1 x 10^4 ~ 1 x 10^6	-7 ~ (-23)
4c	0.73 - 1.01	0.86 ± 0.092	3 x 10^4 ~ 1 x 10^6	-19 ~ (-37)
4d	0.52 - 0.80	0.62 ± 0.10	2 x 10^4 ~ 1 x 10^5	-16 ~ (-32)
4e	0.045 - 0.110	0.077 ± 0.025	2 x 10^3 ~ 1 x 10^5	-19 ~ (-41)

Table 2. Selected Cell Parameters of Single Crystals **4a-4e**

Compound	*a* (Å)	*b* (Å)	*c* (Å)	α (deg.)	β (deg.)	γ (deg.)	Cell Density (g/cm^3)	Space group
4a	11.57	5.13	15.54	90	90.06	90	1.53	P 2$_1$/c
4b	5.07	15.95	25.59	90	90	90	1.45	P bca
4c	11.84	5.08	15.57	90	90.49	90	1.63	P 2$_1$/c
4d	12.40	5.10	16.00	90	95.08	90	1.45	P 2$_1$/c
4e	26.66	6.10	19.32	90	119.16	90	1.30	C 2/c

This journal is © The Royal Society of Chemistry 2015

J. Mater. Chem. C., 2015, **00**, 1-3 | **3**

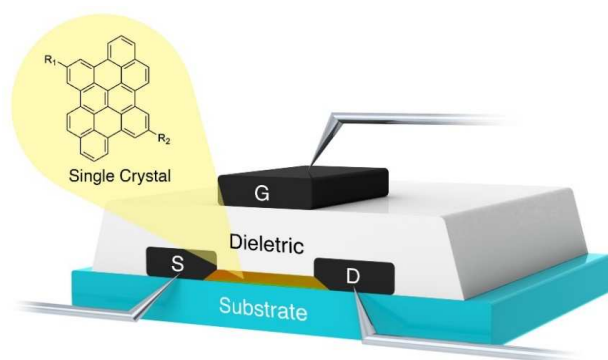**Figure 5.** Schematic diagram of a top-gate SCFET.

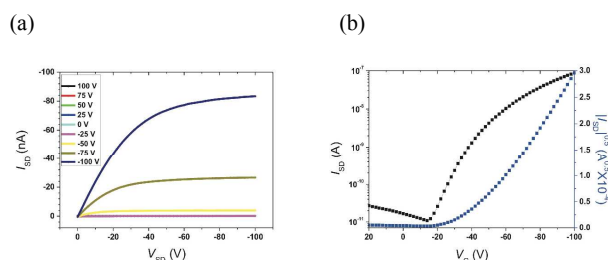(a)   (b)

Figure 6. (a) Output characteristics and (b) transfer characteristics of **4a**.

Theoretical calculations

In order to understand the factors behind the charge mobilities, theoretical computations were performed for molecules **4a-4c** and **4e**. As an asymmetrical derivative, **4d** was not simulated because the intermolecular configurations are not uniquely determined from the crystal structure. For neighbouring pairs of molecules, we calculated the charge hopping rates according to Marcus theory.[19] The mobilities along the π-packing direction are first estimated with the Einstein relationship (μ_E) as listed in Table 4.[20] (details in supplementary information). It is seen that μ_E does not follow the experimental observations: **4e** has the highest theoretical μ_E, whereas the experimental mobility has been the lowest.

Since the electronic coupling is sensitive to the detailed overlap of nodal structures of the molecular orbitals and there are thermal motion for molecules in a crystal,[21] a molecular dynamics (MD) simulation was performed to calculate the averaged coupling $<V_{MD}>$. It is seen that most of the couplings derived from MD increased. For

4e, the averaged coupling for the π-packing pairs becomes 98.2 meV. Therefore, the subsequent mobility derived from the Einstein relationship (data not shown) would still deviate from experimental result.

With the bulky *tert*-butyl substituent in **4e**, there is no herringbone contact in its crystal structure, and the charge-hopping is essentially one-dimensional. Such a character is quite different from other DBBT studied. A system with two or three dimensional hopping network are favourable because the additional dimension offers alternative pathways to move forward without being stopped by a site with low rate. We further simulate the charge mobility with a kinetic Monte Carlo (KMC) scheme, a simulation that allows the charge to move in the 3-dimensional network. The simulated mobility, μ_{KMC}, are as listed Table 4. It is seen that the mobilities all increased in this model, each with a different factor. The mobility for **4e** is increased by a factor of 2.4, relatively small as compared to other molecules, but the overall mobility is still the highest.

In the literature, systems with very large intermolecular coupling are seen with poor mobility performances.[25] In **4e**, the averaged electronic coupling from MD sampling is similar to the reorganization energy λ. Detailed distribution (shown in Figure S5, panel 4e-I of supplementary materials) indicates that more than half of the sampling have their electronic coupling larger than λ. In case with large electronic coupling, it is likely to form delocalized polarons that are energetically lower than other sites and trap the charge.[24] (Figure 7) To include the effect of charge trapping by delocalized, low-energy polarons, we modified the KMC simulation and allowed the charges to be delocalized when the electronic coupling is larger than the reorganization energy. Following details described in the supplemental materials, the final simulated charge mobilities are listed as μ_{deloc} in Table 4. It is seen that **4e** is affected the most, and the simulated mobility drops to 0.0073 cm^2 V^{-1} s^{-1}, while the mobility of other molecules remain in the similar magnitude. This set of results is in general agreement with experimental data. Thus it is believed that the poor performance of **4e**, whose electronic coupling is the largest among the series, is likely due to the existence of delocalized polarons that may serve as traps of the charges. The experimental results are in line with these reports, and with computer simulation we have a possible explanation to this counterintuitive result.

Table 4. Calculated parameters for charge hopping rates and three different theoretical estimates for the charge mobility along the π-stacking direction.

Compound	λ_{in} (meV)	V^{π} ($<V^{\pi}_{MD}>$)[a] (meV)	V^{H} ($<V^{H}_{MD}>$)[b] (meV)	μ_E[d] (cm^{2}V^{-1}s^{-1})	μ_{KMC}[e] (cm^{2}V^{-1}s^{-1})	μ_{deloc}[f] (cm^{2}V^{-1}s^{-1})
4a	100.0	0.2 (22.5)	29.5 (22.4)	0.21	0.71	0.51
4b	126.3	14.9 (40.6)	22.7 (15.1)	0.06	0.37	0.39
4c	117.3	11.0 (27.7)	32.2 (22.2)	0.21	0.69	0.54
4e	103.7	42.0 (98.2)	-[c]	0.77	1.82	0.0073

[a] Electronic coupling for hole-transfer between π-stacked molecules. In the parentheses are averaged values for the MD sampling. [b] Electronic coupling for hole-transfer between herringbone-stacked molecules. In the parentheses are averaged values for the MD sampling. [c] There is no Herringbone-stacked pair in the crystal structure of **4e**. [d] Mobilities estimated using the Einstein's relationship, projected to the π-stacking axis, obtained with V^{π} and V^{H}. [e] Mobilities obtained from a kinetic Monte Carlo simulation, obtained with MD sampled V's. [f] Mobilities obtained from a kinetic Monte Carlo simulation but with delocalized polarons, obtained with MD sampled V's.

$V_{if} \ll \lambda$
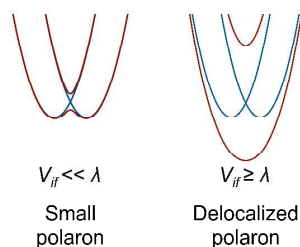Small polaron

$V_{if} \geq \lambda$
Delocalized polaron

Figure 7. When the coupling is larger than the reorganization energy, the charge may be delocalized and form a polaron. Shown are schematic plots for the potential energy curves for the diabatic initial and final states (blue), and the corresponding adiabatic, avoided-crossing states (red).

Experimental Section

General Information

All experimental operations were performed under nitrogen, and the equipment was dried in an oven at 150 °C for several hours. THF and toluene were distilled over sodium particles. CH_2Cl_2 was distilled over calcium hydride. All the other specified chemicals were commercially purchased (ACROS, Aldrich, Alfa and TCI) and used without further purification. ^1H and ^{13}C NMR spectra were measured on either a Bruker AV 400 NMR spectrometer or a Bruker AVANCE 600 NMR spectrometer using $CDCl_3$, CD_2Cl_2 as the solvent. UV/vis absorption spectra were recorded in chlorobenzene (1.0×10^{-5} M) using a Hitachi U-3300 spectrophotometer. HRMS was performed on a Finnigan MAT-95XL High Resolution Mass Spectrometer. Thermogravimetric analysis (TGA) was carried out using a Perkin Elmer Pyris 1 TGA (at a heating rate of 10 ºC per min) and the reported decomposition temperatures represent the temperature observed at 5 % mass loss. The X-ray diffraction was carried out on a Bruker X8APEX X-ray diffractometer with Mo Kα radiation (λ = 0.71073 Å) and the structure was solved by SHELX 97 program. The HOMO levels of the derivatives were measured with a photoelectron spectrometer (AC-2, Riken Keiki) in ambient conditions with a UV source. The LUMO levels were determined by adding to the HOMO level an energy gap determined by UV absorption edge of respective compound.

SCFET Device Fabrication

Top-contact, top-gate SCFET devices were prepared by placing a single crystallite on a glass substrate, which was modified with a monolayer of *n*-octadecyltrichlorosilane (ODTS). Colloidal graphite was used as the source and drain electrodes by painting at both ends of the crystal. A thin film of parylene-N (~2–4 μm thick) was deposited on top of the crystal in a home-made reactor as insulating dielectric. Finally, colloidal graphite was painted on top of the parylene film as the gate electrode. The channel length and width of devices varied depending on the dimensions of the crystal chosen. These parameters, as well as the thickness of parylene, were determined for each individual device. The electrical characteristics of the devices were measured in ambient in a dark chamber using a computer-controlled Agilent 4156C Semiconductor Parameter Analyzer. The field-effect mobility of the OFET devices was

calculated from the I-V characteristics in the saturation region ($I_{SD,sat}$) according to equation 1:[19]

$$I_{SD,sat} = (WC_i/2L)\,\mu_{sat}(V_G - V_{th})^2 \quad (1)$$

where W and L are the channel width and length respectively, and C_i is the capacitance per unit area of the parylene-N insulator, V_G is the gate voltage and V_{th} is the threshold voltage.

Conclusions

In summary, we have synthesized and characterized a new series of planar fused PAHs, namely dibenzo[*de, op*]bistetracene derivatives with symmetrical or unsymmetrical substituent as well as the unsubstituted one by the same convenient route. Substituent not only affects the photophysical and thermal stable properties but also perturbs the packing pattern such that compounds **4a-4d** exhibit shifted π–π stacking and herringbone-packing whereas compound **4e** has just π–π packing because of the size of substituent. SCFET devices were fabricated for all five compounds, which display different charge transfer properties with reasonable correlation by theoretical calculation. The high electronic coupling of **4e** does not lead to higher mobility presumably because the additional traps formed due to delocalized polarons. Among these, the devices with di-methyl substituted **4b** gave a high hole mobility of 1.19 $cm^2V^{-1}s^{-1}$ with a current on/off ratio of up to 10^6.

Acknowledgements

Notes and references

1 (a) C. W. Tang, S. A. VanSlyke, *Appl. Phys. Lett.* 1987, **51**, 913−915. (b) Y. Li, M. K. Fung, Z. Xie, S. T. Lee, L.-S. Hung, J. Shi, *Adv. Mater.* 2002, **14**, 1317−1321. (c) K.-C. Wu; P.-J. Ku, C.-S. Lin, H.-T. Shih, F.-I. Wu, M.-J. Huang, J.-J. Lin, I.-C. Chen, C.-H. Cheng, *Adv. Funct. Mater.* 2008, **18**, 67−75. (d) B. X. Mi, Z. Q. Gao, C. S. Lee, S. T. Lee, H. L. Kwong, N. B. Wong, *Appl. Phys. Lett.* 1999, **75**, 4055−4057. (e) K. M. Omer, S.-Y. Ku, K.-T. Wong, A. J. Bard, *Angew. Chem. Int. Ed.* 2009, **48**, 9300 −9303. (f) J. Xiao, S. Liu, Y. Liu, L. Ji, X. Liu, H. Zhang, X. Sun, Q. Zhang, *Chem. Asian J.* 2012, **7**, 561-564. (g) J. Xiao, H.Yang, Z. Yin, J. Guo, F. Boey, H. Zhang, Q. Zhang, *J. Mater. Chem.* 2011, **21**, 1423–1427. (h) J. Li, Q. Zhang, *Synlett*, 2013, **24**, 686-696.

2 (a) A. Tsumura, H. Koezuka, T. Ando, *Appl. Phys. Lett.*, 1986, **49**, 1210−1212. (b) J. Mei, Y. Diao, A. L. Appleton, L. Fang, Z. Bao, *J. Am.Chem. Soc.* 2013, **135**, 6724−6746. (c) C. Wang, H. Dong, W. Hu, Y. Liu, D. Zhu, *Chem. Rev.* 2012, **112**, 2208–2267. (d) J. E. Anthony, *Angew. Chem. Int. Ed.*

This journal is © The Royal Society of Chemistry 2015

J. Mater. Chem. C, 2015, **00**, 1-3 | **5**

2008, **47**, 452–483. (e) D. T. Chase, A. G. Fix, S. J. Kang, B. D. Rose, C. D. Weber, Y. Zhong, L. N. Zakharov, M. C. Lonergan, C. Nuckolls, M. M. Haley, *J. Am. Chem. Soc.* 2012, **134**, 10349−10352. (f) S. Allard, M. Forster, B. Souharce, H. Thiem, U. Scherf, *Angew. Chem. Int. Ed.* 2008, **47**, 4070–4098. (g) C. Wang, J. Zhang, G. Long, N. Aratani, H. Yamada, Y. Zhao, Q. Zhang, *Angew. Chem Int. Ed.* 2015, **54**, 6292–6296.

3   (a) G. Gelinck, P. Heremans, K. Nomoto, T. D. Anthopoulos, *Adv. Mater.* 2010, **22**, 3778−3798. (b) M. Muccini, *Nat. Mater.* 2006, **5**, 605−613. (c) H. Dong, C. Wang, W. Hu, *Chem. Commun.* 2010, **46**, 5211−5222. (d) H. Klauk, *Chem. Soc. Rev.* 2010, **39**, 2643−2666. (e) A. R. Murphy, J. M. J. Fréchet, *Chem. Rev.* 2007, **107**, 1066−1096. (f) M. E. Roberts, A. N. Sokolov, Z. Bao, *J. Mater. Chem.* 2009, **19**, 3351−3363.

4   (a) V. Podzorov, *MRS Bull.* 2013, **38**, 15−24. (b) R. W. I. de Boer, T. M. Klapwijk, A. F. Morpurgo, *Appl. Phys. Lett.* 2003, **83**, 4345−4347. (c) L. Jiang, H. Dong, W. Hu, *J. Mater. Chem.* 2010, **20**, 4994−5007. (d) R. W. I. de Boer, M. E. Gershenson, A. F. Morpurgo, V. Podzorov, *Phys. Status Solidi A* 2004, **201**, 1302−1331. (e) M. E. Gershenson, V. Podzorov, A. F. Morpurgo, *Rev. Mod. Phys.* 2006, **78**, 973−989. (f) H. Li, B. C. K. Tee, J. J. Cha, Y. Cui, J. W. Chung, S. Y. Lee, Z. Bao, *J. Am. Chem. Soc.* 2012, **134**, 2760−2765. (g) Y.-H. Kim, B. Yoo, J. E. Anthony, S. K. Park, *Adv. Mater.* 2012, **24**, 497−502.

5   V. Coropceanu, J. Cornil, D. A. da Silva, Y. Olivier, R. Silbey, J. L. Bredas, *Chem. Rev.* 2007, **107**, 926–952.

6   Aleshin, A. N.; Lee, J. Y.; Chu, S. W.; Kim, J. S.; Park, Y. W. *Appl. Phys. Lett.* 2004, **84**, 5383−5385.

7   (a) R. W. I. de Boer, T. M. Klapwijk, A. F. Morpurgo, *Appl. Phys. Lett.* 2003, **83**, 4345−4347. (b) C. Reese, W.-J. Chung, M.-m. Ling, M. Roberts, Z. Bao, *Appl. Phys. Lett.* 2006, **89**, 202108.

8   (a) O. D. Jurchescu, M. Popinciuc, B. J. van Wees, T. T. M. Palstra, Adv. Mater. 2007, **19**, 688−692. (b) Y. Takeyama, S. Ono, Y. Matsumoto, *Appl. Phys. Lett.* 2012, **101**, 083303.

9   (a) A. M. v. d. Craats, N. Stutzmann, O. Bunk, M. M. Nielsen, M. Watson, K. Mullen, H. D. Chanzy, H. Sirringhaus, R. H. Friend, *Adv. Mater.* 2003, **15**, 495−499. (b) W. Pisula, A. Menon, M. Stepputat, I. Lieberwirth, U. Kolb, A. Tracz, H. Sirringhaus, T. Pakula, K. Mullen, *Adv. Mater.* 2005, **17**, 684−689. (c) S. Xiao, M. Myers, Q. Miao, S. Sanaur, K. Pang, M. L. Steigerwald, C. Nuckolls, *Angew. Chem., Int. Ed.* 2005, **44**, 7390−7394. (d) X. Zhang, X. Jiang, K. Zhang, L. Mao, J. Luo, C. Chi, H. S. O. Chan, J. Wu, *J. Org. Chem.* 2010, **75**, 8069–8077. (e) S. Pola, C.-H. Kuo, W.-T. Peng, Md. M. Islam, I. Chao, Y.-T. Tao, *Chem. Mater.* 2012, **24**, 2566−2571. (f) C.-H. Kuo, D.-C. Huang, W.-T. Peng, K. Goto, I. Chao, Y.-T. Tao, *J. Mater. Chem. C* 2014, **2**, 3928–3935.

10 (a) K. Senthilkumar, F. C. Grozema, F. M. Bickelhaupt, L. D. A. Siebbeles, *J. Chem. Phys.* 2003, **119**, 9809−9817. (b) Y.

Zhang, D. Hanifi, S. Alvarez, F. Antonio, A. Pun, L. M. Klivansky, A. Hexemer, B. Ma, Y. Liu, *Org. Lett.* 2011, **13**, 6528−6531.

11 (a) A. Lv, S. R. Puniredd, J. Zhang, Z. Li, H. Zhu, W. Jiang, H. Dong, Y. He, L. Jiang, Y. Li, W. Pisula, Q. Meng, W. Hu, Z. Wang, *Adv. Mater.* 2012, **24**, 2626−2630. (b) W. Yue, A. Lv, J. Gao, W. Jiang, L. Hao, C. Li, Y. Li, L. E. Polander, S. Barlow, W. Hu, S. Di Motta, F. Negri, S. R. Marder, Z. Wang, *J. Am. Chem. Soc.* 2012, **134**, 5770−5773.

12 (a) M. G. Schwab, A. Narita, Y. Hernandez, T. Balandina, K. S. Mali, S. De Feyter, X. Feng, K. *J. Am. Chem. Soc.* 2012, **134**, 18169−18172. (b) A.C. Grimsdale, K. Müllen, *Angew. Chem., Int. Ed.* 2005, **44**, 5592−5629. (c) A. Sinitskii, A. Dimiev, D. A. Corley, A. A. Fursina, D. V. Kosynkin, J. M. Tour, *ACS Nano* 2010, **4**, 1949−1954.

13 A. Zinke, R. Ott, *Monatsh. Chem.* 1950, **81**, 1137−1139.

14 T.-A. Chen, R.-S. Liu, *Org. Lett.* 2011, **13**, 4644−4647.

15 N. Miyaura, A. Suzuki, *Chem. Rev.* 1995, **95**, 2457–2483.

16 (a) D. E. Ames, A. Opalko, *Tetrahedron.* 1984, **40**, 1919−1925. (b) E. Jung, K. Park, J. Kim, H.-T. Jung, I.-K. Oh, S. Lee, *Inorg. Chem. Commun.* 2010, **13**, 1329−1331.

17 (a) L. Zhai, R. Shukla, R. Rathore, *Org. Lett.* 2009, **11**, 3474−3477. (b) T. S. Navale, K. Thakur, R. Rathore, *Org. Lett.* 2011, **13**, 1634−1637.

18 R. A. Laudise, C. Kloc, P. G. Simpkins, T. Siegrist, *J. Cryst. Growth* 1998, **187**, 449−454.

19 R. A. Marcus, N. Sutin, *Biochim. Biophys. Acta* 1985, **811**, 265−322.

20 W.-Q. Deng, W. A. Goddard, *J. Phys. Chem. B* 2004, **108**, 8614−8621.

21 (a) D. Beljonne, G. Pourtois, C. Silva, E. Hennebicq, L. M. Herz, R. H. Friend, G. D. Scholes, S. Setayesh, K. Müllen, J. L. Brédas, *Proc. Natl Acad. Sci.* 2002, **99**, 10982−10987. (b) B.-C. Lin, C.-P. Cheng, Z.-Q. You, C.-P. Hsu, *Phys. Chem. Chem. Phys.* 2011, **13**, 20704−20713.

22 S.-H. Wen, A. Li, J. Song, W.-Q. Deng, K.-L. Han, W. A. Goddard, *J. Phys. Chem. B* 2009, **113**, 8813−8819.

23 H. Bassler, *Phys. Status. Solidi. B* 1993, **175**, 15−56.

24 R. P. Fornari, A. Troisi, *Adv. Mater.* 2014, **26**, 7627−7631.

25 (a) B. R. Kaafarani, T. Kondo, J. Yu, Q. Zhang, D. Dattilo, C. Risko, S. C. Jones, S. Barlow, B. Domercq, F. Amy, A. Kahn, J.-L. Brédas, B. Kippelen, S. R. Marder *J. Am. Chem. Soc.* 2005, **127**, 16358−16359. (b) V. Lemaur, D. A. da Silva Filho, V. Coropceanu, M. Lehmann, Y. Geerts, J. Piris, M. G. Debije, A. M. van de Craats, K. Senthilkumar, L. D. A. Siebbeles, J. M. Warman, J.-L. Brédas, J. Cornil, *J. Am. Chem. Soc.* 2004, **126**, 3271−3279. (c) I. Yavuz, B. N. Martin, J. Park, K. N. Houk, *J. Am. Chem. Soc,* 2015, **137**, 2856−2866.

26 S. M. Sze, *Semiconductor Device Physics and Technology, 2nd ed.* Wiley, New York, 2001, Chap. 6, p. 169.

6 | *J. Mater. Chem. C.*, 2015, **00**, 1-3

This journal is © The Royal Society of Chemistry 2015

Table of Content

A series of five dibenzo[*de, op*]bistetracene derivatives is synthesized in short steps and their single-crystal field-effect transistor devices show a hole mobility from 0.045 cm^2 V^{-1} s^{-1} up to 1.19 cm^2 V^{-1} s^{-1}, due to the effect of substituents on the crystal packing/electronic coupling.